Diffusion Path of Oxide Ions in an Apatite-Type Ionic Conductor $La_{9.69}(Si_{5.70}Mg_{0.30})O_{26.24}$

Roushown Ali,[†,‡,§] Masatomo Yashima,*[,‡] Yoshitaka Matsushita,[†,||] Hideki Yoshioka,[⊥] Kenji Ohoyama,[#] and Fujio Izumi[†]

Quantum Beam Center, National Institute for Materials Science, 1-1 Namiki, Tsukuba, Ibaraki 305-0044, Japan, Department of Materials Science and Engineering, Interdisciplinary Graduate School of Science and Engineering, Tokyo Institute of Technology, 4259 Nagatsuta-cho, Midori-ku, Yokohama, 226-8502, Japan, Hyogo Prefectural Institute of Technology, 3-1-12 Yukihira-cho, Suma-ku, Kobe 654-0037, Japan, and Institute for Materials Research, Tohoku University, Katahira 2-1-1, Aoba-ku, Sendai 980-8577, Japan

Received December 10, 2007. Revised Manuscript Received June 8, 2008

Densities of coherent-scattering lengths in oxide-ion conductor $La_{9.69}(Si_{5.70}Mg_{0.30})O_{26.24}$ with an apatite-type structure (space group $P6_3/m$) have been determined by a whole-pattern fitting approach based on the maximum-entropy method (MEM) using neutron powder diffraction data measured at 25 and 1558 °C. The Rietveld refinement suggested an interstitial oxygen (O5) atom site (12*i*; *x*, *y*, *z*; $x \approx 0$, $y \approx 0.22$, $z \approx 0.65$) at the periphery of the hexagonal axis. The oxide ions located at 2*a* (O4) and 12*i* (O3) sites are largely distributed parallel and perpendicular to the *c* axis, respectively. The densities of coherent-scattering lengths derived from the MEM analysis revealed that the O4 oxide ions located at the 2*a* site (0, 0, 1/4) diffuse to nearest-neighbor 2*a* sites along the [001] direction. This [001] diffusion path is linearly linked with that of neighboring unit cell, which forms a long-range, one-dimensional oxide-ion diffusion pathway extending along the *c* axis of the hexagonal $P6_3/m$ framework. The probability density of the O3 ion is connected with that of the equivalent O3 of the same tetrahedron through the interstitial O5 ion, indicating migration of the ions along a curved line connecting O3−O5−O3 atoms. This migration path is nonlinear (U-shaped) and perpendicular to the *c* axis. The densities of the two kinds of oxide ions (O4 and O3) migrating parallel and perpendicular to the *c* axis, respectively, connected with each other through the densities of interstitial oxide ion (O5). The results suggest that the O4 ion migrates via vacancy mechanism with a direct linear path along the *c* axis, while the O3 ion migration perpendicular to the *c* axis involves an interstitial mechanism.

Introduction

Solid oxides exhibiting high ionic conductivity have been the subject of considerable research interest. In particular, the oxide-ion conductors are useful materials for fuel cells, catalysts, gas sensors and batteries.[1–6] Improving our understanding of ionic transport behavior in materials with high oxide-ion diffusivity and relating the crystal structure of these materials to ionic conductivity have become fundamentally important to the design and development of new oxide-ion conductors. This has motivated the extensive study of many oxide-ion conductors over the last few decades.[4] Recently, there has been significant interest in Si-based materials having an apatite-type structure because of higher oxide-ion conductivities at middle temperature range below 700 °C.[5,7]

A large number of experimental and atomistic simulation studies have been conducted to investigate the crystal structure and ion-migration pathway in apatite-type rare earth silicates $Ln_{10-x}Si_6O_{26\pm\delta}$ (Ln = lanthanides) and doped variants where x and δ are the deviations of Ln and O

* To whom all correspondence should be addressed. E-mail: yashima@materia.titech.ac.jp.
† National Institute for Materials Science.
‡ Tokyo Institute of Technology.
§ Permanent address: Department of Chemistry, University of Rajshahi, Rajshahi-6205, Bangladesh.
|| Present address: Beam line BL15XU, SPring-8, NIMS-branch office, 1-1-1 Kohto, Sayo-cho, Hyogo 679-5148.
⊥ Hyogo Prefectural Institute of Technology.
Tohoku University.

(1) Higuchi, M.; Masubuchi, Y.; Nakayama, S.; Kikkawa, S.; Kodaira, K. *Solid State Ionics* **2004**, *174*, 73–80.
(2) Nakayama, S.; Aono, H.; Sadaoka, Y. *Chem. Lett.* **1995**, *6*, 431–432.
(3) Lacorre, P.; Goutenoire, F.; Bohnke, O.; Retoux, R.; Laligant, Y. *Nature* **2000**, *404*, 856–858.
(4) Boivin, J. C.; Mairesse, G. *Chem. Mater.* **1998**, *10*, 2870–2888.
(5) Nakayama, S.; Sakamoto, M. *J. Eur. Ceram. Soc.* **1998**, *18*, 1413–1418.
(6) Nakayama, S.; Higuchi, M. *J. Mater. Sci. Lett.* **2001**, *20*, 913–915.
(7) Nakayama, S.; Sakamoto, M.; Highchi, M.; Kodaira, K. *J. Mater. Sci. Lett* **20001**, *19*, 91–93.
(8) Islam, M. S.; Tolchard, J. R.; Slater, P. R. *Chem. Commun.* **2003**, 1486–1487.
(9) Tolchard, J. R.; Islam, M. S.; Slater, P. R. *J. Mater. Chem.* **2003**, *13*, 1956–1961.
(10) Tolchard, J. R.; Sansom, J. E. H.; Islam, M. S.; Slater, P. R. *Dalton Trans.* **2005**, *20*, 1273–1280.
(11) (a) Yoshioka, H. *Chem. Lett.* **2004**, *33*, 392–393. (b) Yoshioka, H. *J. Am. Ceram. Soc.* **2007**, *90*, 3099–3105.
(12) Kendrick, E.; Sansom, J. E. H.; Tolchard, J. R.; Islam, M. S.; Slater, P. R. *Faraday Discuss.* **2007**, *134*, 181–194.
(13) Yoshioka, H.; Tanase, S. *Solid State Ionics* **2005**, *176*, 2395–2398.
(14) Leon-Reina, L.; Porras-Vazquez, J. M.; Losilla, E. R.; Aranda, M. A. G. *Solid State Ionics* **2006**, *177*, 1307–1315.

10.1021/cm7035234 CCC: $40.75
Published on Web 07/22/2008

concentrations from nominal compositions.[1,8–20] The space group of the oxyapatites is typically $P6_3/m$.[1,7,18–20] Two kinds of diffusion pathways—a direct linear path along the hexagonal *c* axis and a nonlinear, sinusoidal-like path through interstitial oxide ions—have been proposed in the literature.[8,9,17–19] However, these diffusion paths have not been determined directly from experiments.

Among many rare earth oxyapatites, $La_{10-x}Si_6O_{26+\delta}$ are some of the promising compounds exhibiting significant oxide-ion conductivity. Their conductivity is reported to increase largely by the incorporation of excess oxygen (i.e., $\delta > 0$).[17] The conductivity of the oxyapatites increases by substituting Mg for Si atoms.[11–13] Therefore, this study focuses on apatite-type Mg-doped lanthanum silicate with excess oxygen $La_{9.69}(Si_{5.70}Mg_{0.30})O_{26.24}$.

Experimental data at lower temperature do not provide enough information to identify atomistic mechanisms of ionic diffusion pathways, because the mobile ions are localized. Information on the diffusion path and structural disorder of mobile oxide ions at high temperatures, where the materials work most efficiently, is indispensable for developing better oxide-ion conductors. A combined technique of Rietveld analysis, maximum-entropy method (MEM),[21] and MEM-based pattern fitting (MPF)[22,23] is expected to be effective for determining the spatial distribution of mobile oxide ions.[24–26] In this research, the crystal structure and pathway of oxide-ion diffusion of $La_{9.69}(Si_{5.70}Mg_{0.30})O_{26.24}$ are investigated at 25 and 1558 °C by employing this technique for neutron powder diffraction data. Neutron diffractometry is utilized for the following reasons: (1) the relatively high contributions of oxygen atoms to diffraction intensities in $La_{9.69}(Si_{5.70}Mg_{0.30})O_{26.24}$ containing heavy-metal atoms and (2) the ease of collecting quality diffraction data at 1558 °C.

Experimental Section

A $La_{9.69}(Si_{5.70}Mg_{0.30})O_{26.24}$ sample was prepared by solid-state reactions from high-purity powders of La_2O_3, SiO_2, and MgO previously heated at 1000 °C for 4 h. The powders were mixed in appropriate ratios, ground with ethanol, and calcined at 1300 °C for 16 h. The calcined powders were further ground, pressed into disks, and sintered at 1600 °C for 4 h. The first sintering produced porous disks because of high reactivity of the calcined powders with atmospheric H_2O and CO_2. Therefore, they were reground, pressed into disks, and sintered again at 1750 °C for 8 h on MgO-stabilized-ZrO_2 setters placed inside a $MoSi_2$ furnace, resulting in dense ceramic disks with a diameter of ~13 mm and a thickness of ~1 mm. One of the sintered disks was crushed and ground into a powder for use in laboratory-based X-ray powder diffraction measurements. Chemical analysis identified the composition as $La_{9.692(4)}(Si_{5.700(1)}Mg_{0.303(1)})O_{26.242(8)}$. The homogeneity of the sample was confirmed by synchrotron powder diffraction measurements at 25 °C at the beam line BL-$4B_2$ of Photon Factory, KEK, Japan.[27] A second harmonic generation (SHG) measurement for $La_{9.71}(Si_{5.8}Mg_{0.2})O_{26.37}$ was carried out to examine whether the material has a center of symmetry or not. The SHG measurement was done by powder method with a Nd:YAG laser operated at a wavelength of 1064 nm, which was used as the radiation source with an irradiation time of 8 s. The laser power was 300 μJ. The sample was ground to the grain size of about 1 to 2 μm in order to avoid the possible influence of domain structure and phase-matching conditions.

Neutron powder diffraction experiments of $La_{9.69}(Si_{5.70}Mg_{0.30})O_{26.24}$ were performed in air at 25 and 1558 °C using a powder diffractometer, HERMES, installed at the JRR-3 M research reactor of the Japan Atomic Energy Agency.[28] Incident neutrons with a fixed wavelength of 1.8265(1) Å were obtained using a vertically focusing (331) Ge monochromator. Diffraction data were collected in the 2θ range from 3° to 153° using 150 ^{3}He counters. A furnace with molybdenum silicide heaters was used to heat the $La_{9.69}(Si_{5.70}Mg_{0.30})O_{26.24}$ sample during data collection.[29] The temperature of the sample was maintained within ±1.5 °C during the measurement.

The neutron diffraction data were analyzed by the Rietveld method followed by application of MEM and MPF using the computer programs RIETAN-FP[30] and PRIMA.[21] Diffraction data in the 2θ range of 6.0−130°, corresponding to $d > 1.0$ Å (where *d* is the spacing of lattice planes), were used in the Rietveld and MPF analyses. A split-type pseudo-Voigt profile function formulated by Toraya[31] was used in the Rietveld refinements. The cutoff value was 7.00 × (full-width at half-maximum). Background intensities were fit using a Legendre polynomial function with 12 parameters. Anisotropic atomic displacement parameters (U_{ij}) with an anisotropic Debye−Waller factor (=exp[$-2\pi^2(h^2a^{*2}U_{11} + k^2b^{*2}U_{22} + l^2c^{*2}U_{33} + 2hka^*b^*U_{12} + 2hla^*c^*U_{13} + 2klb^*c^*U_{23}$)]) were assigned to all cation and anion sites, except the interstitial site. The coherent scattering lengths (b_c) adopted for Rietveld

(15) Lambert, S.; Vincent, A.; Bruneton, E.; Beaudet-Savignat, S.; Guillet, F.; Minot, B.; Bouree, F. *J. Solid State Chem.* **2006**, *179*, 2602–2608.
(16) Sansom, J. E. H.; Kendrick, E.; Tolchard, J. R.; Islam, M. S.; Slater, P. R. *J. Solid State Electrochem.* **2006**, *10*, 562–568.
(17) (a) Slater, P. R.; Sansom, J. E. H.; Tolchard, J. R. *Chem. Rec.* **2004**, *4*, 373–384. (b) Kendrick, E.; Islam, M. S.; Slater, P. R. *J. Mater. Chem.* **2007**, *17*, 3104–3111.
(18) Leon-Reina, L.; Losilla, E. R.; Martinez-Lara, M.; Bruque, S.; Llobet, A.; Sheptyakov, D. V.; Aranda, M. A. G. *J. Mater. Chem.* **2005**, *15*, 2489–2498.
(19) Leon-Reina, L.; Losilla, E. R.; Martinez-Lara, M.; Bruque, S.; Aranda, M. A. G. *J. Mater. Chem.* **2004**, *14*, 1142–1149.
(20) (a) Masubuchi, Y.; Higuchi, M.; Takeda, T.; Kikkawa, S. *Solid State Ionics* **2006**, *177*, 263–268. (b) Okudera, H.; Masubuchi, Y.; Kikkawa, S.; Yoshiasa, A. *Solid State Ionics* **2005**, *176*, 1473–1478. (c) Iwata, T.; Fukuda, K.; Béchade, E.; Masson, O.; Julien, I.; Champion, E.; Thomas, P. *Solid State Ionics* **2007**, *178*, 1523–1529.
(21) Izumi, F.; Dilanian, R. A. *Recent Research Developments in Physics*; Transworld Research Network: Trivandrum, India, 2002; Vol. 3, Part II, pp 699−726.
(22) Izumi, F.; Kumazawa, S.; Ikeda, T.; Hu, W.-Z.; Yamamoto, A.; Oikawa, K. *Mater. Sci. Forum* **2001**, *378−381*, 59–64.
(23) Izumi, F. *Solid State Ionics* **2004**, *172*, 1–6.
(24) (a) Yashima, M.; Nomura, K.; Kageyama, H.; Miyazaki, Y.; Chitose, N.; Adachi, K. *Chem. Phys. Lett.* **2003**, *380*, 391–396. (b) Ali, R.; Yashima, M.; Izumi, F. *Chem. Mater.* **2007**, *19*, 3260–3264. (c) Yashima, M.; Enoki, M.; Wakita, T.; Ali, R.; Matsushita, Y.; Izumi, F.; Ishihara, T. *J. Am. Chem. Soc.* **2008**, *139*, 2762–2763. (d) Yashima, M.; Itoh, M.; Inaguma, Y.; Morii, Y. *J. Am. Chem. Soc.* **2005**, *127*, 3491–3495. (e) Yashima, M.; Kamioika, T. *Solid State Ionics* **2008**, *179*, 1939–1943. (f) Yashima, M.; Tsuji, T. *J. Appl. Crystallogr.* **2007**, *40*, 1166–1168.
(25) (a) Yashima, M.; Ishimura, D. *Chem. Phys. Lett.* **2003**, *378*, 395–399. (b) Yashima, M.; Ishimura, D. *Appl. Phys. Lett.* **2005**, *87*, 221909. (3 pages). (c) Yashima, M.; Xu, Q.; Yoshiasa, A.; Wada, S. *J. Mater. Chem.* **2006**, *16*, 4393–4396.
(26) (a) Yashima, M.; Kobayashi, S.; Yasui, T. *Faraday Discuss.* **2007**, *134*, 369–376. (b) Yashima, M.; Kobayashi, S. *Appl. Phys. Lett.* **2004**, *84*, 526–528. (c) Yashima, M.; Kobayashi, S.; Yasuda, T. *Solid State Ionics* **2006**, *84*, 526–528. (d) Wakita, T.; Yashima, M. *Appl. Phys. Lett.* **2008**, *92*, 101921-1–101921-3.
(27) Toraya, H.; Hibino, H.; Ohsumi, H. *J. Synchrotron Radiat.* **1996**, *3*, 75–84.
(28) Ohoyama, K.; Kanouchi, T.; Nemoto, K.; Ohashi, M.; Kajitani, T.; Yamaguchi, Y. *Jpn. J. Appl. Phys.* **1998**, *37* (Part 1), 3319–3326.
(29) Yashima, M. *J. Am. Ceram. Soc.* **2002**, *85*, 2925–2930.
(30) Izumi, F.; Momma, K. *Solid State Phenom.* **2007**, *130*, 15–20.
(31) Toraya, H. *J. Appl. Crystallogr.* **1990**, *23*, 485–491.

Table 1. Refined Crystal Parameters, Anisotropic Atomic Displacement Parameters, and Reliability Indices of the $La_{9.69}(Si_{5.70}Mg_{0.30})O_{26.24}$

temp.	atom	site	g	x	y	z	U_{11} (Å^2)	U_{22} (Å^2)	U_{33} (Å^2)	U_{12} (Å^2)	U_{13} (Å^2)	U_{23} (Å^2)	U_{eq} (Å^2)
25 °C	La1	4*f*	0.923	1/3	2/3	−0.0007(4)	0.005(1)	U_{11}	0.016(2)	0.5* U_{11}	0.0	0.0	0.008
1558 °C	La1	4*f*	0.923	1/3	2/3	−0.0007(7)	0.037(2)	U_{11}	0.040(3)	0.5* U_{11}	0.0	0.0	0.038
25 °C	La2	6*h*	1.0	0.0115(3)	0.2397(3)	1/4	0.006(2)	0.006(1)	0.009(1)	0.004(1)	0.0	0.0	0.007
1558 °C	La2	6*h*	1.0	0.0128(5)	0.2394(4)	1/4	0.037(3)	0.035(3)	0.042(2)	0.016(2)	0.0	0.0	0.039
25 °C	SiMg	6*h*	1.0	0.4023(4)	0.3721(5)	1/4							0.006(1)
1558 °C	SiMg	6*h*	1.0	0.4018(7)	0.3749(7)	1/4	0.026(4)	0.020(4)	0.048(4)	0.014(3)	0.0	0.0	0.030
25 °C	O1	6*h*	1.0	0.3238(4)	0.4864(4)	1/4	0.025(2)	0.027(3)	0.015(2)	0.023(2)	0.0	0.0	0.018
1558 °C	O1	6*h*	1.0	0.3273(7)	0.4881(8)	1/4	0.096(5)	0.077(6)	0.079(5)	0.068(5)	0.0	0.0	0.073
25 °C	O2	6*h*	1.0	0.5980(4)	0.4733(4)	1/4	0.009(2)	0.016(2)	0.016(2)	0.007(2)	0.0	0.0	0.013
1558 °C	O2	6*h*	1.0	0.5894(5)	0.4677(7)	1/4	0.043(4)	0.069(4)	0.076(6)	0.030(4)	0.0	0.0	0.061
25 °C	O3	12*i*	1.0	0.3469(3)	0.2561(3)	0.0685(3)	0.039(2)	0.019(2)	0.011(1)	0.018(1)	−0.014(1)	−0.004(9)	0.022
1558 °C	O3	12*i*	1.0	0.3446(5)	0.2613(5)	0.0708(5)	0.132(5)	0.061(3)	0.052(3)	0.042(3)	−0.041(3)	−0.023(2)	0.084
25 °C	O4	2*a*	0.96(2)	0.0	0.0	1/4	0.006(3)	U_{11}	0.20(1)	0.5* U_{11}	0.0	0.0	0.070
1558 °C	O4	2*a*	0.98(2)	0.0	0.0	1/4	0.058(7)	U_{11}	0.42(2)	0.5* U_{11}	0.0	0.0	0.178
25 °C	O5	12*i*	0.026	−0.004(9)	0.24(1)	0.60(1)							0.013
1558 °C	O5	12*i*	0.023	0.03(2)	0.20(1)	0.70(2)							0.051

25 °C	cell parameters	$a = 9.7303(3)$ Å, $c = 7.2082(2)$ Å
1558 °C		$a = 9.8773(7)$ Å, $c = 7.2982(4)$ Å

25 °C	reliability factors[a]	$R_{wp} = 4.17\%$, $R_p = 2.96\%$, $S = 5.41$, $R_I = 0.73\%$, $R_F = 0.34\%$
1558 °C		$R_{wp} = 2.97\%$, $R_p = 2.24\%$, $S = 3.31$, $R_I = 1.60\%$, $R_F = 1.00\%$
25 °C	reliability factors[b]	$R_I = 0.71\%$, $R_F = 0.31\%$
1558 °C		$R_I = 0.98\%$, $R_F = 0.60\%$

[a] Reliability factors in the Rietveld analysis. [b] Reliability factors in the MEM-based pattern fittings.

refinement were 8.24 fm for La, 4.149 fm for Si, 5.375 fm for Mg, and 5.805 fm for O.

MEM analysis was conducted using the 219 structure factors obtained from Rietveld analysis, with the unit cell divided into 100 × 100 × 80 pixels. The 100 reflection appearing at the lowest 2θ position (ca. 12°) was included in the MEM analysis, as that peak provides information on the disordered arrangements of oxide ions. The iterative procedure, REMEDY cycle,[21,22] was employed after the MEM analyses to reduce the nuclear-density bias imposed by the structural models adopted in the Rietveld analyses. Use of the REMEDY cycle resulted in significant improvement in the reliability indices based on the Bragg intensities (R_I) and structure factors (R_F; Table 1). The nuclear density obtained after the REMEDY cycle was drawn with VESTA program.[32]

Results and Discussion

(1) Refinement of Crystal Structure of $La_{9.69}(Si_{5.70}Mg_{0.30})O_{26.24}$. All the reflections in the neutron and synchrotron powder diffraction profiles of $La_{9.69}(Si_{5.70}Mg_{0.30})O_{26.24}$ were indexed with a hexagonal cell ($a = b = 9.7303(3)$ Å and $c = 7.2082(2)$ Å at 25 °C; $a = b = 9.8773(7)$ Å, $c = 7.2982(4)$ Å at 1558 °C, $\alpha = \beta = 90°$, and $\gamma = 120°$). In accordance with earlier reports,[1,9,10,15,18] the rare earth silicates and germanates belong to hexagonal space group $P6_3/m$, $P\bar{3}$ or $P6_3$. The space group $P6_3/m$ has a center of symmetry while the $P6_3$ does not. The SHG measurement of $La_{9.71}(Si_{5.81}Mg_{0.18})O_{26.37}$ showed no signal, which indicates that $La_{9.71}(Si_{5.81}Mg_{0.18})O_{26.37}$ has a center of symmetry. Therefore, the noncentrosymmetric space group $P6_3$ is ruled out for the present $La_{9.69}(Si_{5.70}Mg_{0.30})O_{26.24}$ sample. The $P\bar{3}$ symmetry can be excluded for this structure because it has lower symmetry compared with $P6_3/m$. Therefore, $P6_3/m$ is the correct space group for $La_{9.69}(Si_{5.70}Mg_{0.30})O_{26.24}$.

Rietveld analysis of the neutron powder diffraction data of $La_{9.69}(Si_{5.70}Mg_{0.30})O_{26.24}$ measured at 25 and 1558 °C was performed on the basis of hexagonal $P6_3/m$. The Si and Mg atoms were assumed to occupy the same site, and occupancies of the atoms were fixed at the values derived from the chemical analysis (Table 1). In a preliminary analysis the site occupancies of La1 and La2 atoms, namely, g(La1) and g(La2), were refined. The La2 site was determined to be fully occupied, whereas the La1 site was about 93% occupied. Refinement of oxygen occupancy factors resulted in a small amount of vacancies (3%) only for the 2*a* site, whereas all other oxygen sites were fully occupied. Oxygen O5 atoms were placed at an interstitial site (12*i*) near the hexagonal *c* axis as was proposed in the literature,[9,18,19] and Rietveld refinement gave the fractional coordinates (−0.004(9), 0.24(1), 0.60(1)) at 25 °C and (0.03(2), 0.20(1), 0.70(2)) at 1558 °C. The values obtained at 25 °C are in good agreement with those reported in the literatures.[9,18,19] The distances between O3 and O5 atoms were short (Table 2); however, when O5 atom is present locally, the silicate tetrahedron is translated/rotated, and these distances are longer as discussed

Table 2. Selected Interatomic Distances (Å) for $La_{9.69}(Si_{5.70}Mg_{0.30})O_{26.24}$ at 25 °C and 1558 °C

	25 °C	1558 °C
La1−O1 × 3	2.487(3)	2.521(6)
La1−O2 × 3	2.538(4)	2.582(6)
La1−O3 × 3	2.854(3)	2.937(5)
⟨La1−O⟩	2.626	2.680
La2−O1	2.775(5)	2.838(9)
La2−O2	2.518(4)	2.621(7)
La2−O3 × 2	2.480(2)	2.515(4)
La2−O3 × 2	2.611(4)	2.692(6)
La2−O4	2.278(2)	2.304(3)
⟨La2−O⟩	2.532	2.594
Si,Mg−O1	1.634(6)	1.617(9)
Si,Mg−O2	1.650(4)	1.605(7)
Si,Mg−O3 × 2	1.634(3)	1.629(5)
<Si,Mg−O>	1.639	1.617
O5−Si,Mg	1.78(8)	1.9(1)
O5−O3	1.0(1)	1.5(1)
O3−O3	5.252(4)	5.328(6)
La2−La2	3.946(3)	3.991(5)

(32) Momma, K.; Izumi, F. *J. Appl. Crystallogr.* **2008**, *41*, 653–658.

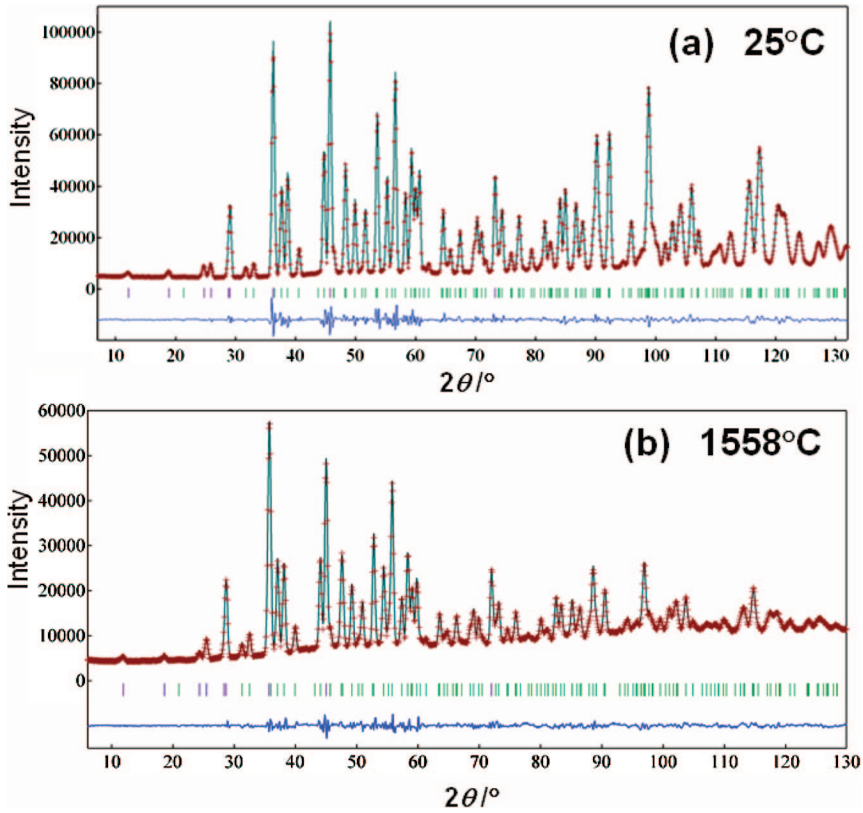

Figure 1. Rietveld fitting pattern for $La_{9.69}(Si_{5.70}Mg_{0.30})O_{26.24}$ at (a) 25 °C and (b) 1558 °C. Crosses and lines denote observed and calculated profile intensities, respectively. Short vertical bars represent Bragg reflection positions. The difference (observed − calculated) is plotted below each profile.

in the literature.[8,9,19] Such positional disorder in the silicate tetrahedron is shown later in the present MEM nuclear density maps. The number of O5 atoms per formula unit was estimated to be 0.30 from the chemical composition and charge neutrality, leading to the occupancy factors of O5 site to be 0.026 and 0.023 at 25 and 1558 °C, respectively. We fixed the occupancy factors of oxygen atoms at the O5 site to be 0.026 and 0.023 at 25 and 1558 °C, respectively, in the final refinements. The final refinements were performed using anisotropic atomic displacement parameters (U_{ij}) for all anions and cations, except interstitial oxygen (O5) at 1558 °C, and $Si_{0.95}Mg_{0.05}$ and (O5) at 25 °C. This model gave a fairly large anisotropic atomic displacement parameter U_{33}(O4), which suggests oxide-ion diffusion along the *c* axis. Thermal motion of O5 atom was assumed to be isotropic because of its small occupancy (Table 1). The technique of partial profile relaxation[21,24a] was applied to 10 reflections with profiles broadening anisotropically. The resulting calculated pattern agreed well with the observed one (Figure 1). Final crystallographic parameters and reliability indices are listed in Table 1.

The positions of all cations and anions were almost independent of temperature, except the interstitial oxygen O5 anion (Table 1). The atomic displacement parameters of oxide ions were larger than those of the cations, suggesting a larger diffusion coefficient for oxide ions. The oxygen atoms O3 and O4 displayed large anisotropy in the atomic displacement parameters (Table 1 and Figure 2a,c). The atomic displacement parameters at 1558 °C were larger than those at 25 °C, which indicates the larger dynamic disorder, thermal motions, and atomic movements at higher temperature of 1558 °C.

Figure 2a,c shows the crystal structures of $La_{9.69}(Si_{5.70}Mg_{0.30})O_{26.24}$ drawn with the refined crystallographic parameters at 25 and 1558 °C, respectively. The structure consists of six isolated $[Si_{0.95}Mg_{0.05}O_4]$ tetrahedra in the hexagonal unit cell, and each tetrahedron contains three kinds of fully occupied oxygen atoms (O1, O2, and O3). The remaining oxygen atoms mainly occupy the O4 site on the hexagonal axis, whereas a few oxygen (O5) atoms lie midway between the tetrahedron and the O4 atom.

We did not detect any symmetry change between 25 and 1558 °C. The refined crystal structure of $La_{9.69}(Si_{5.70}Mg_{0.30})O_{26.24}$ at 25 °C is similar with that reported for Al- and Mg-doped and nondoped lanthanum silicates.[11b,14,18,19] The lattice parameters (Table 1) obtained at 25 °C are in good agreement with those ($a = 9.73415(1)$ and $c = 7.21605(2)$ Å; $a = 9.725$ Å and $c = 7.208$ Å) for $La_{9.67}(Si_{5.5}Mg_{0.5})O_{26}$[12] and $La_{9.6}(Si_{5.70}Mg_{0.30})O_{26.1}$,[13] respectively. Compared with nondoped $La_{9.33}Si_6O_{26}$.[18] the lattice parameters obtained in the present study are a little higher, which is ascribed to the partial substitution of Mg (having higher ionic radius) for the Si site. At a higher temperature of 1558 °C, the *y* coordinate of the O5 atom approached the hexagonal *c* axis, while the *z* coordinate became closer to the O4 atom. A similar trend was observed for the $La_{9.33}(SiO_4)_6O_2$ compound.[18] The interatomic distances obtained from the present refined crystal structure at 25 °C (Table 2) are in agreement with those of $La_{9.67}(Si_{5.5}Mg_{0.5})O_{26}$[12] and $La_{9.33}(SiO_4)_6O_2$.[18] With increasing temperature the bond distances of La1—O

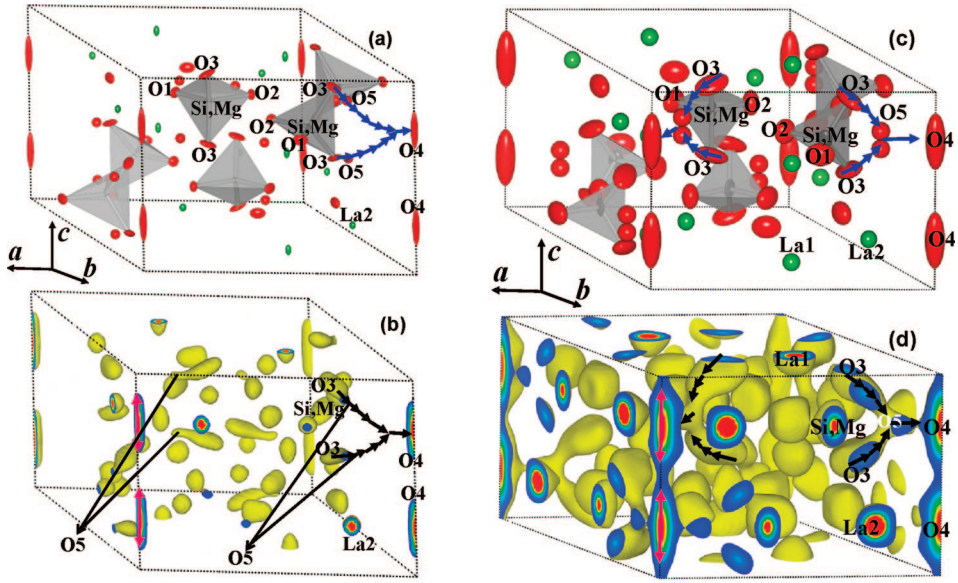

Figure 2. Refined crystal structure of $La_{9.69}(Si_{5.70}Mg_{0.30})O_{26.24}$ at (a) 25 °C and (c) 1558 °C. Oxygen atoms (O3) which are members of the $(Si_{0.95}Mg_{0.05})O_4$ tetrahedron migrate to the oxygen atoms (O4) located at the hexagonal axis through the interstitial oxygen (O5) following a curved path (black arrows). (b and d) Equicontour surface of the scattering amplitude distribution. Red arrows indicate a direct linear diffusion pathway of the oxide ions.

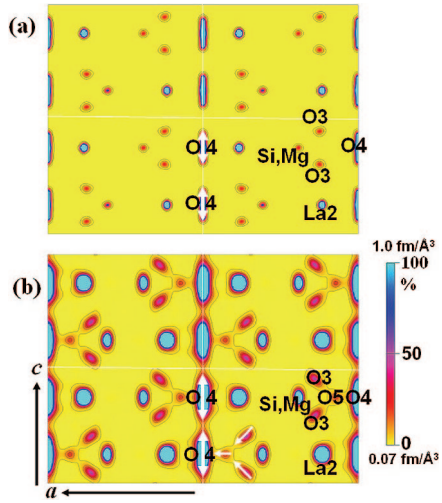

Figure 3. Scattering amplitude distribution on (010) plane of the $La_{9.69}(Si_{5.70}Mg_{0.30})O_{26.24}$ at (a) 25 °C and (b) 1558 °C with contours in the range from 0.07 to 1.0 fm $Å^{-3}$ (step 0.2 fm $Å^{-3}$). At 25 °C density of O5 is very close to that of O3 and is not resolved.

and La2−O increase while Si,Mg−O distances decrease slightly, which is also consistent with the literature.[18]

(2) Nuclear Density Distribution and Oxide-Ion Conduction of $La_{9.69}(Si_{5.70}Mg_{0.30})O_{26.24}$. Figures 2b,d and 4b show the isosurfaces of nuclear densities in the $La_{9.69}(Si_{5.70}Mg_{0.30})O_{26.24}$. The nuclear density contour map from $y = 0.0$ to $y = 0.01$ projected onto the (010) plane is shown in Figure 3. Figures 2b,d, 3, and 4b provide information on the positional disorder and diffusion path of the mobile oxide ions compared to the simple atomistic model (Figures 2a,c and 4a).

The nuclear density distributions and their isosurfaces (Figures 2d, 3b, and 4b) show three kinds of diffusion paths: (1) a linear O4−O4 diffusion pathway along the *c* axis, (2) an O4−O5 path along the *a* axis, and (3) a curved O5−O3 path. An O4 atom is coupled with three O4−O5−O3

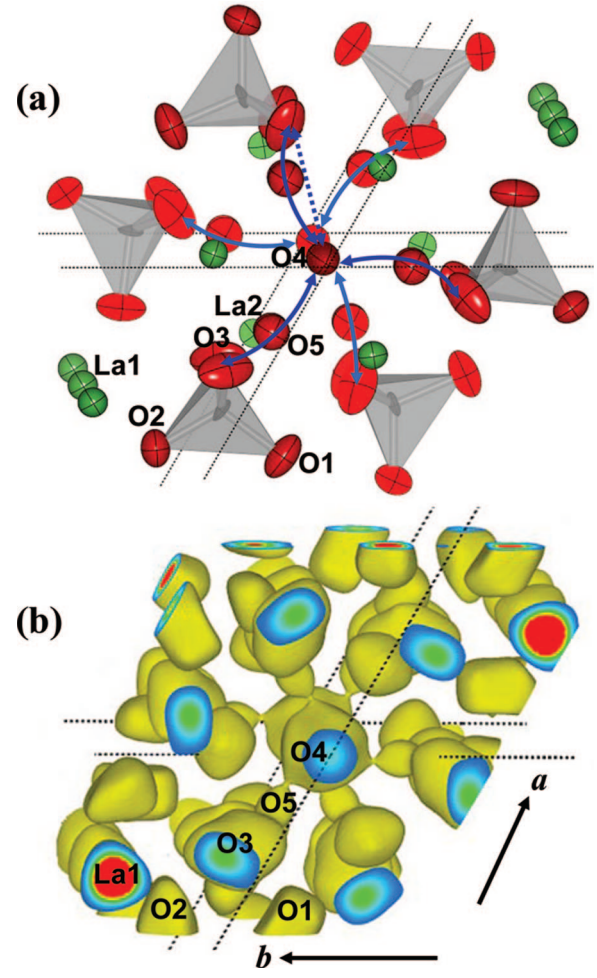

Figure 4. (a) Atomic arrangement of $La_{9.69}(Si_{5.70}Mg_{0.30})O_{26.24}$ at 1558 °C around the hexagonal axis. The deep and light red colors represent atoms lying at upper and lower layers, respectively. Deep and light blue arrows indicate migration pathway of upper and layers, respectively. (b) Equicontour surface of the scattering amplitude distribution around the hexagonal axis at 0.15 fm $Å^{-3}$.

migrating paths (Figure 4). The O4 oxide ions located at the 2*a* (0, 0, 1/4) site on the hexagonal *c* axis have a large distribution along the ⟨001⟩ direction. The densities of the O4 atoms are connected with those of nearest-neighbor O4 atoms, which shows a diffusion pathway parallel to the *c* axis. The O4 atoms migrate linearly to the nearest-neighbor O4 and followed a long-range, one-dimensional diffusion path along the *c* axis. The nuclear-density distribution indicates diffusion pathway along the *c* axis not only when the refinement is performed with anisotropic thermal displacement parameter but also when the refinement is performed with isotropic thermal displacement parameter of O4 atom. The probability densities of O3 atoms were largely distributed perpendicular to the *c* axis and connected with those of another O3 atom in the same tetrahedron via those of the interstitial O5 atom, which indicates a short-range movement among the O3−O5−O3 atoms (Figure 2d). This migration path is nonlinear (U-shaped). The probability densities of two kinds of oxygen atoms O4 and O3 migrating parallel and perpendicular to the *c* axis, respectively, connect with each other through the densities of interstitial O5 atom.

The saddle point of the diffusion path along the *c* axis lies between two O4 atoms. This diffusion path is direct and linear because there are no ions to affect the direction of the linear pathway along the *c* axis (Figure 4). At 1558 °C the oxide-ion migration paths along the lines connecting O3−O5 and O5−O4 atoms are clearly visualized in the density distribution (Figures 2d and 3b). At the midway between O3 and O5 atoms the density of the coherent scattering length is 0.30 fm Å^{-3}, whereas it is 0.17 fm Å^{-3} between O5 and O4. The O3 ions migrate to the 2*a* site (O4) through the interstitial site (O5) following a curved path to maintain a relatively constant distance from cations La2 (solid arrows in Figure 4a), rather than a direct linear path (straight dotted arrow between regular positions in Figure 4a). In many other structural families, the migration pathway running between equivalent atoms is curved,[24–26] whereas in the present apatite-type structure, migrating atoms follow a curved route connecting three nonequivalent atoms (O3−O5−O4). The O3−O5−O4 diffusion paths can be connected through an O2 atom, leading to oxide-ion migration perpendicular to the *c* axis.

In the present work, we have observed two migration pathways. One linear pathway (−O4−O4−) is parallel to the *c* axis, while the other (O3−O5−O4−O5−O3) is perpendicular to the *c* axis. The former is connected across the unit cells, although the latter is not. Thus, the O4 ions located at the hexagonal *c* axis are the main migrating oxide ions, and the pathway lies in the hexagonal channel of the $P6_3/m$ framework. These results are consistent with the conductivity studies[1,6,7] of apatite-type single crystals $Re_{9.33}(SiO_4)_6O_2$ (Re = Pr, Nd, Sm). Those studies demonstrated that the conductivity component parallel to the *c* axis is higher by about 1 order of magnitude than the perpendicular component. Previous reports in atomistic simulation and neutron diffraction studies[8,9,18,19] have suggested that the interstitial oxide ions migrate with a nonlinear path along the *c* axis without involving oxide ions located at the hexagonal axis (O4 in Figure 2). Here, we have found the interstitial oxide ions (O5) to be a connecting point between the O4 (located at hexagonal axis) and O3 (member of tetrahedron) oxide ions. The O4, O5, and O3 ions form diffusion paths perpendicular to the *c* axis. Therefore, the interstitial oxygen atoms would increase the oxide-ion diffusion perpendicular to the *c* axis in an apatite-type structure. This is consistent with high ionic conductivity in apatite-type phases with the oxygen excess.[17b]

Compared to nondoped $La_{9.33}(SiO_4)_6O_2$,[18] the present compound $La_{9.69}(Si_{5.70}Mg_{0.30})O_{26.24}$ (Mg doping on Si site) shows an expansion of unit cell parameters. The Si,Mg−O1, Si,Mg−O2, Si,Mg−O3 bond distances of the present $La_{9.69}(Si_{5.70}Mg_{0.30})O_{26.24}$ are higher than those of $La_{9.33}(SiO_4)_6O_2$,[18] which indicate an expansion of $[Si_{0.95}Mg_{0.05}O_4]$ tetrahedra. The expansion of tetrahedral coordination sphere by doping Mg on Si site would improve the ionic conductivity. Similar speculation of enhancing the ionic conduction by doping Mg on the Si site was also done by Yoshioka[11b] and Kendrick et al.[12] The O4 atoms migrate along the *c* axis through a triangle formed by O3 atoms (O3−O3−O3). This is the conduction channel by which the oxide ion (O4) can go through. Substitution of Mg^{2+} ion (having higher ionic radius and lower valence) for Si site increases the size of O3−O3−O3 triangle. At 25 °C the bond distance O3−O3 obtained in the present study is 5.252(4) Å, which is little higher than that reported for nondoped lanthanum silicate $La_{9.33}Si_6O_{26}$[18] (5.212(3) Å) and $La_{9.55}Si_6O_{26.32}$[19] (5.2486(12) Å). An increase of the size of O3−O3−O3 triangle indicates the expansion of the conduction channel which enhances the migration of O4 atoms to the nearest-neighbor O4 along the *c* axis. The migration of O4 ion occurs through a vacancy mechanism. The nonlinear migration of O3−O5−O4−O5−O3 atoms is via an interstitial mechanism. The oxygen excess introduces oxygen atoms at the interstitial site (O5), which also enhances the conductivity. Diffusion pathways in simple perovskite- and fluorite-type structures have been visualized in the past,[24–26] whereas here the diffusion pathway for a complicated apatite-type structure is visualized for the first time.

Acknowledgment. The authors thank the authority of JAEA for use of the neutron powder diffractometer. We would like to thank Mr. K. Nemoto for the use of the HERMES diffractometer. Special thanks are extended to Mr. T. Wakita, Mr. T. Tsuji, and Mr. Y. Kawaike for experimental assistance. We thank Dr. M. Nakamura and Mr. S. Takenouchi (NIMS) for their helps with SHG and ICP measurements, respectively. This research was supported in part by the Ministry of Education, Culture, Sports, Science and Technology of Japan (Monbu-Kagaku-sho). The neutron and synchrotron powder diffraction experiments were performed under the user programs of no. 7769 and no. 2004G256 of Photon Factory, respectively.

CM7035234